Geological Society of America
3300 Penrose Place
P.O. Box 9140
Boulder, CO 80301
(303) 447-2020 • fax 303-357-1073
www.geosociety.org

Geological Society of America
Special Paper 396
2005

Deformation of flow bands by bubbles and crystals

Michael Manga[†]
Department of Earth and Planetary Science, University of California at Berkeley, Berkeley, California 94720-4767, USA

ABSTRACT

Bands in volcanic rocks are deformed by inclusions, such as bubbles and crystals. The shape of deformed bands is compared with theoretical models for flow around inclusions. Deformation through either simple or pure shear can be distinguished for phenocrysts, but not bubbles. Studying band deformation at the microscale thus complements other textural measurements and structural approaches for reconstructing the kinematics and dynamics of lava flows.

Keywords: inclusion, flowband, strain path, lava flow.

INTRODUCTION

Flow banding is pervasive in silicic lava flows and domes. The use of the word "flow" in the term "flow band" implies that the geometry of bands is caused by deformation of the lava as it flows. Bands, such as those shown in Figure 1, can be defined by variations in bulk or trace element composition, crystallinity, or vesicularity. Several different processes can lead to the formation of bands, including magma mingling (e.g., Seaman, 1995; Perugini et al., 2004), welding and rheomorphism (e.g., Stevenson et al., 1993), and repeated autobrecciation followed by reannealing (e.g., Smith, 1996; Gonnermann and Manga, 2003; Tuffen et al., 2003). Regardless of the origin of the bands, their presence in lavas provides a tracer to study lava deformation. The kinematics and dynamics inferred from studying bands, however, may be used to test models for band formation (e.g., Gonnermann and Manga, 2005).

One common feature of flow bands is that they are thinned and curved in the vicinity of inclusions, such as bubbles and crystals. These contortions of bands should provide insight into the flow experienced by the bands. Similar structures develop from compaction, deformation, and recrystallization in metamorphic rocks and are reflected in foliations and lineations. In a metamorphic rock, to model the formation of structures, coupled equations for fluid and solid deformation, as well as mass transfer between solid and fluid phases, should be solved (e.g., McKenzie and Holness, 2000). In contrast, in lava, flow in the vicinity of inclusions is governed by the much simpler problem of incompressible viscous flow.

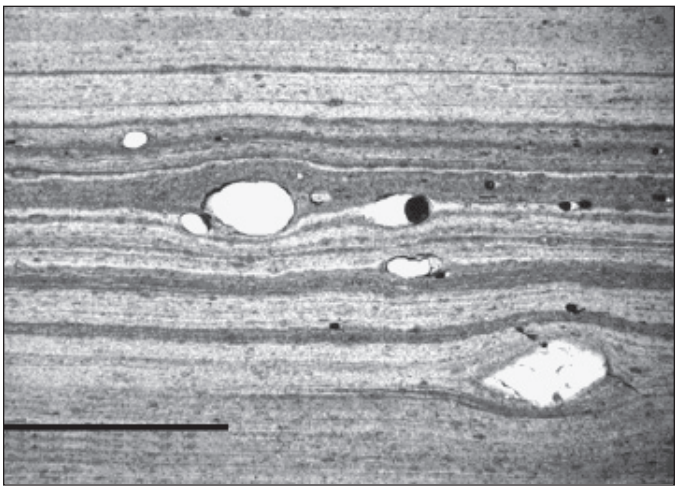

Figure 1. Bands in obsidian from Big Obsidian Flow, Newberry Volcano (Oregon, USA) from Castro (1999). Scale bar is 1 mm long. The ellipsoidal inclusions are bubbles. The phenocryst in the lower right is feldspar.

[†]E-mail: manga@seismo.berkeley.edu.

Manga, M., 2005, Deformation of flow bands by bubbles and crystals, *in* Manga, M., and Ventura, G., eds., Kinematics and dynamics of lava flows: Geological Society of America Special Paper 396, p. 47–53. doi: 10.1130/2005.2396(04).

Here I examine flow bands in obsidian to identify features of flow dynamics and kinematics that can be recovered from the deformation of bands through their interaction with spherical inclusions in the lava. I show, for example, that it is possible to distinguish between pure (coaxial) and simple shear (an example of noncoaxial) flow.

SAMPLES

The obsidian samples studied in this article are from Obsidian Dome (California, USA), Little Glass Mountain (California, USA), and Rock Mesa (Oregon, USA). Obsidian Dome and Little Glass Mountain are effusive obsidian flows that erupted ca. 0.5 ka (Miller, 1985) and 1.1 ka (Donnelly-Nolan et al., 1990), respectively. The Rock Mesa sample is from a 2.2 ka pyroclastic fall deposit on the flanks of South Sister Volcano, Oregon, USA (Scott, 1987).

Thin sections are cut parallel to the inferred flow direction and perpendicular to the plane of banding (i.e., flow bands define planes that are perpendicular to the thin section). The flow direction is estimated from the orientation of elongate phenocrysts and microlites, deformed bubbles, and macroscopic foliations.

I focus on obsidian for two reasons. First, the optical transparency of the glass permits straightforward measurement and imaging of structures (Castro et al., 2003). Second, the concentration of crystals and bubbles is often sufficiently low that the interactions between the bubbles and crystals can be neglected, which greatly simplifies the quantitative analysis of preserved structures. The extension to flows with higher crystallinity, although in principle straightforward, requires both more challenging measurements (e.g., Gray et al., 2003) and more complex theoretical models to account for more complex rheology (e.g., Smith, 2000) and particle interactions (e.g., Arbaret et al., 1996).

GOVERNING EQUATIONS

I assume that, at the length scales for flow around the inclusions, deformation of lava is Newtonian. Flow is then governed by the Stokes equations

$$\nabla p_d = \mu \nabla^2 \mathbf{u} \text{ and } \nabla \cdot \mathbf{u} = 0 \tag{1}$$

with boundary conditions

$$\mathbf{u} \to \mathbf{u}_{\text{ext}} \text{ as } \mathbf{x} \to \infty. \tag{2}$$

Here, p_d is the dynamic pressure, μ the fluid viscosity, $\mathbf{u}$ the fluid velocity, and $\mathbf{x}$ a position vector defined relative to the center of the inclusion, as shown in Figure 2. Bold symbols indicate vector and tensor quantities. The Newtonian approximation is reasonable provided strain rates are one to two orders of magnitude less than those for the glass transition (Webb and Dingwell, 1990), the relevant length scales of flow are comparable to or smaller than the distance between bubbles (Manga et al., 1998), and crystallinities are sufficiently low (less than 1% in this case) so that they do not form an interconnected and rigid network (e.g., Saar et al., 2001).

Inclusions such as bubbles and phenocrysts provide obstacles to the free flow and deformation of magma. As a consequence, bands will be deformed around such inclusions, and the deformation of these bands depends on properties of the flow. We will assume that the external flow in equation 2, $\mathbf{u}_{\text{ext}}$, is a linear flow; that is

$$\mathbf{u}_{\text{ext}} = \boldsymbol{\Gamma} \cdot \mathbf{x} = \mathbf{E} \cdot \mathbf{x} + \frac{1}{2}\boldsymbol{\omega} \times \mathbf{x} \tag{3}$$

where $\boldsymbol{\Gamma}$ is the velocity gradient tensor, $\mathbf{E}$ is the rate-of-strain tensor, and $\boldsymbol{\omega}$ characterizes the vorticity of the external flow. The solution for the flow velocity $\mathbf{u}$ at position $\mathbf{x}$ from the center of an isolated spherical particle or bubble can be derived most easily using vector harmonic methods (see, for example, Leal, 1992)

$$\mathbf{u} = \mathbf{E} \cdot \mathbf{x} + \frac{1}{2}(\boldsymbol{\omega} \times \mathbf{x}) + \alpha\left(\frac{2\mathbf{E} \cdot \mathbf{x}}{5|\mathbf{x}|^5} - \frac{5\mathbf{x}(\mathbf{x} \cdot \mathbf{E} \cdot \mathbf{x})}{|\mathbf{x}|^7}\right) - \beta\frac{\mathbf{x}(\mathbf{x} \cdot \mathbf{E} \cdot \mathbf{x})}{|\mathbf{x}|^5} \tag{4}$$

For a bubble, $\alpha = 1$ and $\beta = 1$, and for a rigid sphere, $\alpha = -1/2$ and $\beta = 5/2$. Although deformed bubbles are common (e.g., Fig. 1) and phenocrysts are not spherical, the derivation of theoretical results is much more complex for nonspherical inclusions.

For completeness the pressure p and stress tensor $\mathbf{T}$ are given, respectively, by

$$p(\mathbf{x}) = p_{\text{ext}} - 2\beta\mu\frac{\mathbf{x} \cdot \mathbf{E} \cdot \mathbf{x}}{|\mathbf{x}|^5} \tag{5}$$

and

$$\begin{aligned}\mathbf{T}(\mathbf{x}) = -p_{\text{ext}}\mathbf{I} + 2\mu\mathbf{E} + \alpha\mu\Bigg[4\frac{\mathbf{E}}{|\mathbf{x}|^5} - \frac{10}{|\mathbf{x}|^7}\big[2\mathbf{x}(\mathbf{E} \cdot \mathbf{x}) + 2(\mathbf{E} \cdot \mathbf{x})\mathbf{x} \\ + (\mathbf{x} \cdot \mathbf{E} \cdot \mathbf{x})\mathbf{I}\big] + \frac{70}{|\mathbf{x}|^9}(\mathbf{x} \cdot \mathbf{E} \cdot \mathbf{x})\mathbf{x}\mathbf{x}\Bigg] \\ - 2\beta\mu\left[\frac{\mathbf{x}(\mathbf{E} \cdot \mathbf{x}) + (\mathbf{E} \cdot \mathbf{x})\mathbf{x}}{|\mathbf{x}|^5} - \frac{5}{|\mathbf{x}|^7}(\mathbf{x} \cdot \mathbf{E} \cdot \mathbf{x})\mathbf{x}\mathbf{x}\right]\end{aligned} \tag{6}$$

Here p_{ext} denotes the pressure far away from the inclusion ($\mathbf{x} \to \infty$), and $\mathbf{I}$ is the identity matrix.

For the illustrative examples considered next, we consider two end member cases of linear flows shown in Figure 3: simple shear and pure shear. Because both the governing equations and external flow are linear, any combination of these flows can be

superposed by linearly adding the solutions. For a simple shear flow, with

$\mathbf{u}_{ext} = (u_x, u_y, u_z) = (Gy, 0, 0)$, we have

$$\mathbf{E} = \begin{pmatrix} 0 & G/2 & 0 \\ G/2 & 0 & 0 \\ 0 & 0 & 0 \end{pmatrix} \text{ and } \boldsymbol{\omega} = (0,0,-G). \quad (7)$$

For a two-dimensional pure shear flow, with $\mathbf{u}_{ext} = (u_x, u_y, u_z) = (Hx,-Hy,0)$, we have

$$\mathbf{E} = \begin{pmatrix} H & 0 & 0 \\ 0 & -H & 0 \\ 0 & 0 & 0 \end{pmatrix} \text{ and } \boldsymbol{\omega} = \mathbf{0}. \quad (8)$$

In the examples that follow, I show the expected shape of bands formed by flow around inclusions. The calculated bands are shown as sets of curves, the shape of which can be compared with actual bands. The calculated bands are determined by advecting material lines that initially start far from the inclusions and by following these material lines through the flow (that is, I integrate $d\mathbf{X}/dt$, where $\mathbf{X}$ describes the position of a material line at time t). In the case of simple shear, calculated bands will be the same as streamlines.

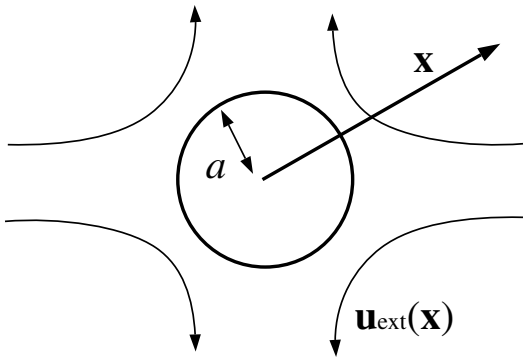

Figure 2. Geometry of the model flow problem showing the inclusion (bubble or rigid sphere). Here a is the inclusion radius, **x** indicates position and $\mathbf{u}_{ext}(\mathbf{x})$ external flows.

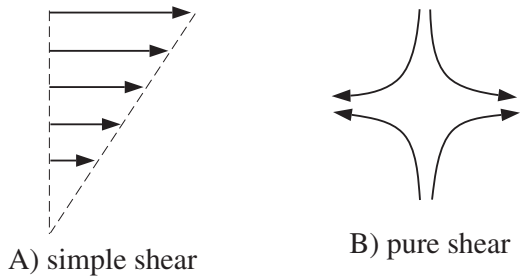

Figure 3. Illustration of flow lines for pure shear (A) and simple shear (B).

PHENOCRYSTS

Figure 4 shows deformed bands of microlites around a phenocryst in obsidian from Obsidian Dome. Also shown are streamlines for pure (solid curves) and simple (dashed curves) shear around a rigid sphere. For the case of simple shear, the sphere is allowed to rotate freely. Predicted band shapes for pure shear agree much better with the observed deformed bands. The difference between these two flows is greatest just upstream (and downstream) of the sphere, and for this reason, I only show predicted band shapes close to the sphere for the simple shear case. This sample was collected from the front of the flow in an obsidian layer located approximately midway between the base and surface of the flow. Here, flow is expected to be dominated by pure shear (Merle, 1998), as inferred from Figure 4. Castro et al. (2002) analyzed the orientation distribution of the microlites in Obsidian Dome and also concluded that flow in the same obsidian layer was probably dominated by pure shear.

Figure 5 shows oriented microlites around a phenocryst in obsidian from Little Glass Mountain. Also shown are calculated shapes of deformed bands for different proportions of pure and simple shear around a rigid sphere, assuming again that the sphere is free to rotate. The relative proportions of pure and simple shear change from all pure shear (Fig. 5A) to all simple shear (Fig. 5C) with equal amounts of pure and simple shear in Fig. 5B. A qualitative comparison of the calculated and observed flow bands indicates a combination of pure and simple shear. The

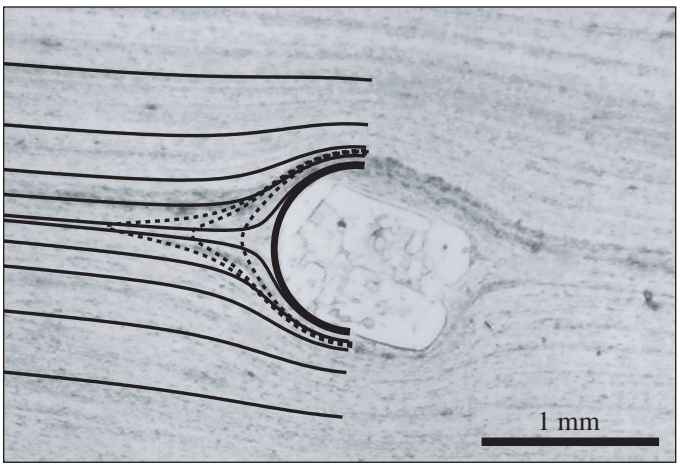

Figure 4. Bands in obsidian from Obsidian Dome, California, USA, deformed by a phenocryst. Predicted deformation of bands for pure shear (solid curves) and simple shear (dashed curves) around a rigid sphere (bold, solid semicircle). Deformation of bands is better explained by pure shear than simple shear.

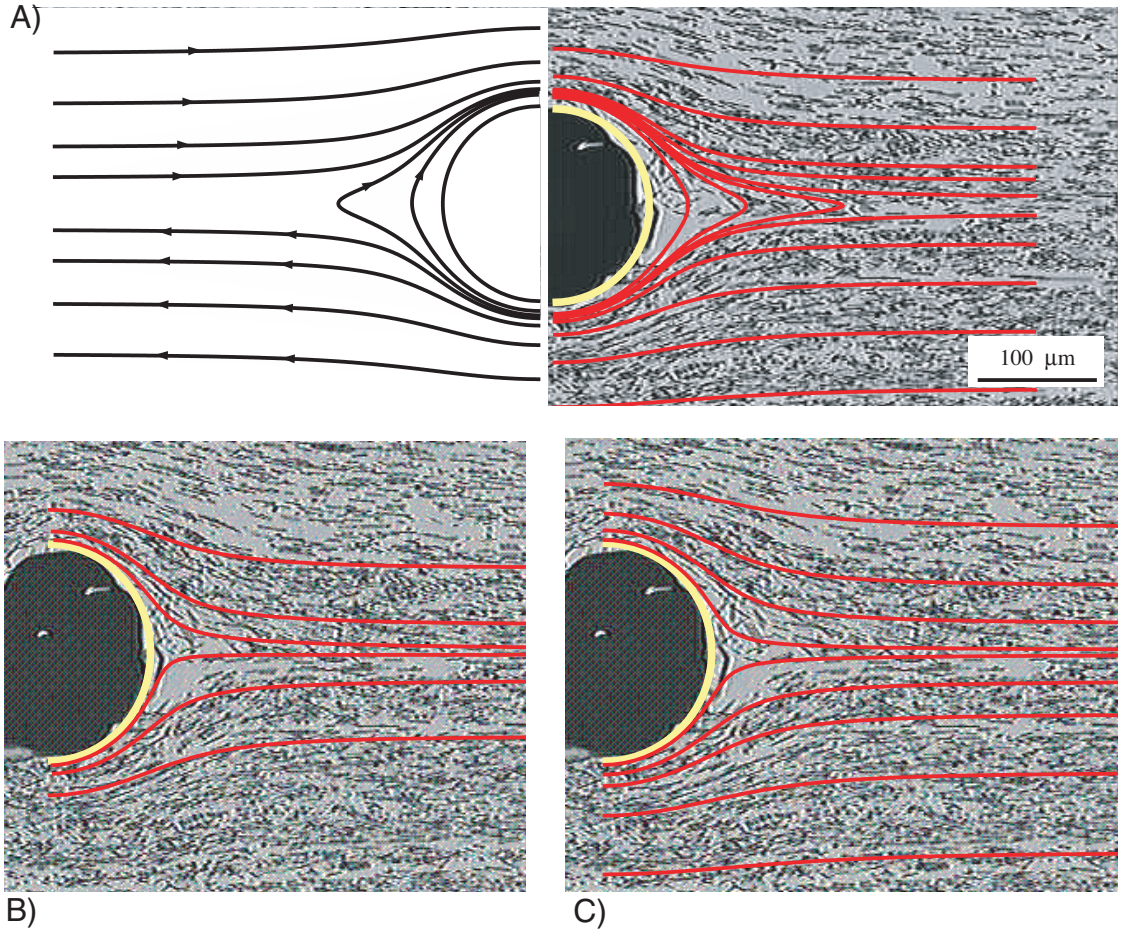

Figure 5. A band deformed by flow around a phenocryst from Obsidian Dome, California, USA, showing changes in microlite orientation. Also shown in (A) are expected shapes of deformed bands (parallel to the expected orientation of microlites) for simple shear around a sphere. (B) Predicted band shapes for a flow that consists of equal parts pure and simple shear, that is G and H in equations 7 and 8 are identical. (C) Predicted band shapes for a flow that consists only of pure shear. Thick yellow semicircle shows the assumed boundary between the phenocryst and glass.

difference between the two end members is most obvious close to the phenocryst, in the region often termed a "stress shadow." This sample was collected from the front and near the base of the flow. At the very bottom of a flow, deformation is expected to be dominated by simple shear because of the no-slip boundary condition on the bottom of the flow. The relative amount of pure shear increases upward from the base (Buisson and Merle, 2004). The conclusion that some pure shear is preserved differs from my earlier analysis (Manga, 1998), in which I showed that the orientation distribution of microlites in the same sample is better explained by simple shear than by pure shear. One possible explanation for this discrepancy is that the orientation distribution of microlites developed in the conduit (where flow should be dominated by simple shear). The size and number density of microlites in the conduit are not much different from those at the flow front, suggesting that most microlites have formed prior to the lava flowing over the surface (Castro et al., 2002). Once on the surface, the pure shear associated with spreading is then more rapidly reflected in the band shapes than in the microlite orientations. The orientation distribution of microlites preserved in these rocks requires strains of order 10 to develop. In contrast, strains of order 1 are sufficient for band deformation to reliably indicate the type of flow.

BUBBLES

Bubbles, unlike solid phenocrysts, may themselves be sources of lava deformation in an otherwise stagnant lava if they grow as a result of exsolution or shrink because of resorption. The growth of bubbles within extruding silicic domes and flows is one way for lavas to develop high vesicularities. Whether bubbles grow within the flow to make vesicular pumice with large bubbles (e.g., Fink et al., 1992)—the so-called coarse vesicular pumice—or bubbles are reabsorbed or collapsed to make low-vesicularity obsidian (e.g., Eichelberger et al., 1986) has been the subject of some controversy.

The flow created by an expanding bubble, when the influence of other bubbles can be ignored, is given by

$$\mathbf{u}(\mathbf{x}) = \left(\frac{a}{|x|}\right)^2 \frac{da}{dr}\mathbf{e}_x \quad (9)$$

where a is the radius of the bubble and $\mathbf{e}_x$ is a unit vector in the same direction as $\mathbf{x}$.

Figure 6 shows deformed bands around a bubble in obsidian from Obsidian Dome. Also shown are the expected shapes of initially planar and parallel bands that are displaced outward by the growing bubble. The agreement between the observed and calculated band deformations suggests that this bubble grew after the bands were created, and thus presumably after emplacement of the lava, that is, after the lava had ceased moving.

Identical deformed bands, however, are also produced by both simple and pure shear around a spherical (nondeforming) bubble. The reason all these flows produce the same deformed bands is that the velocity field responsible for band deformation (i.e., the disturbance flow) in all cases is that created by a point force, or Stokeslet. The disturbance in the flow created by a rigid sphere, in contrast, is more complicated because of the no-slip boundary condition on the surface of the sphere, and it differs for pure and simple shear flows. As a consequence, for our spherical bubble, we can confirm that flow bands are indeed flow bands, in that they reflect flow and deformation, but we cannot be more specific about the nature of the flow without additional constraints.

DISCUSSION

Bands are formed by deformation of ascending and flowing magma and thus preserve a record of this deformation. As with all geological structures, the geometry of the bands we are left to analyze reflects the integrated history of their formation and subsequent deformation, and some care and thought is needed to interpret any observations.

In order for strain to be smoothly distributed in a lava containing rigid phenocrysts or spherical bubbles, the melt must undergo higher strain in the vicinity of inclusions, which results in the observed contortion of bands. The selected examples were chosen because they illustrate that it is possible to infer flow type (e.g., pure vs. simple shear), at least when the concentration of inclusions is low. To determine an increment of strain, an initial shape or position of the material that defines bands must be known. Unfortunately, for the examples considered here, the total strain could thus not be determined. In addition, without knowing the time over which deformation occurs, deformed bands do not contain information about strain rate.

To reconstruct the full kinematics and dynamics from structural and textural measurements clearly requires other measurements. Table 1 provides a summary of the kinematic and dynamic properties (flow type, strain rate, total strain) that can be determined quantitatively from textural and structural studies. The symbols Y, N, and S indicate whether the listed structure can, cannot, or can only sometimes be used to determine the listed kinematic and dynamic properties. Deformed bubbles, because of the presence of surface tension stresses, can in some cases be used to determine either deformation rates or strain, as well as flow type (Coward, 1980; Polacci and Papale, 1997; Rust et al., 2003). Deformed enclaves provide constraints on total strain and flow type (Williams and Tobisch, 1994; Blake and Fink, 2000; Ventura, 2001), provided the rheology and formation of the enclaves are understood (Paterson et al., 2004; Holtz et al., 2004). The preferred orientation of crystals, and the resulting fabrics, reflect both the flow type and total strain (e.g., Shelley, 1985; Wada, 1992; Ventura

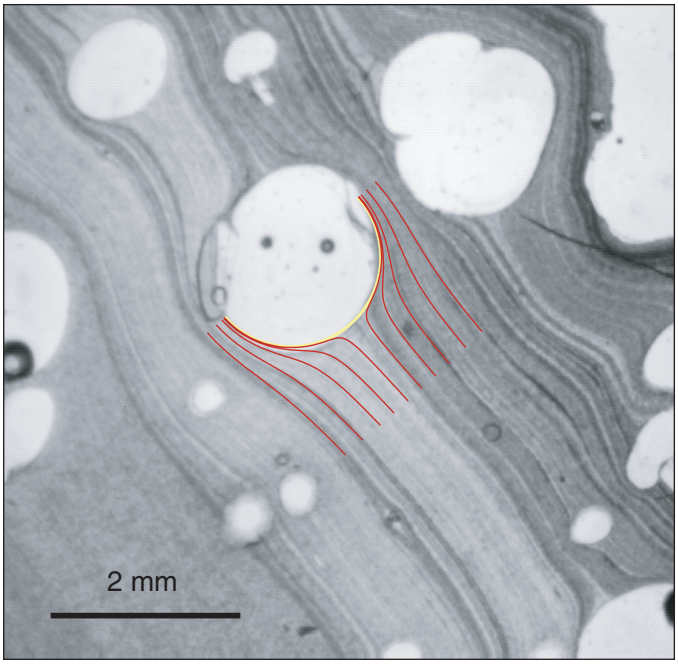

Figure 6. Predicted deformation of bands (red curves) around an expanding bubble. Identical band deformation is also produced by pure and simple shear around a spherical bubble. Sample is from Obsidian Dome, California, USA. Thick yellow semicircle shows the assumed boundary between the bubble and glass.

TABLE 1. FLOW ATTRIBUTES THAT CAN BE QUANTIFIED FROM DIFFERENT STRUCTURES

Structure	Strain	Strain rate	Flow type
Bubbles	S	S	S
Enclaves	Y	N	Y
Crystals	S	N	S
Folds	Y	N	Y
Bands	S	N	S

Note: S—sometimes; Y—yes; N—no.

et al., 1996; Manga, 1998; Smith, 2002). Finally, the shape of folds can reflect the flow type and strain (e.g., Fink, 1980; Smith and Houston, 1994; Castro and Cashman, 1999), provided the rheology of the different layers in the fold is known (e.g., Biot, 1961; Schmalholz and Podladchikov, 2000). In Table 1, I assign an S for strain inferred from bands, because if the initial conditions can be reconstructed, strain can then be inferred.

Table 1 shows that several sets of studies are needed to reconstruct flow dynamics and kinematics. Fortunately, Table 1 also shows that there is likely to be independent confirmation of inferences based on only one type of measurement. For example, in the examples shown in Figures 4 and 5, the orientation distribution of microlites provides an independent check on the flow type inferred from the deformed bands.

As a further example, in Figure 7A I show deformation of a band of oxide particles around a much larger clump of oxides in a sample of pyroclastic obsidian from Rock Mesa, Oregon. This obsidian is assumed to come from near the conduit wall, where flow is most likely dominated by simple shear (Rust et al., 2003). In Figure 7B, I superimpose a flow line for a simple shear flow around a sphere (representing the large clump of oxide particles); the agreement is excellent, indicating that flow was dominated by simple shear. Confirmation is provided by the deformed bubbles at the top of the image in Figure 7B; in simple shear, deformed bubbles are oriented at an angle to the flow direction. This angle depends on the magnitude of deformation (Rust and Manga, 2002), and the orientation of the bubble in Figure 7B is consistent with the flow direction that can be inferred from the line of oxide particles.

Figure 7B, however, also shows the expected shape of a band deformed by pure shear around the same clump of oxide particles. Its shape is nearly identical to the shape of the band formed in simple shear. As noted in Figure 4, the difference between bands deformed in pure and simple shear is most apparent just upstream and downstream of inclusions. As a consequence, to interpret deformed bands, it is essential to focus on their shapes very close to inclusions.

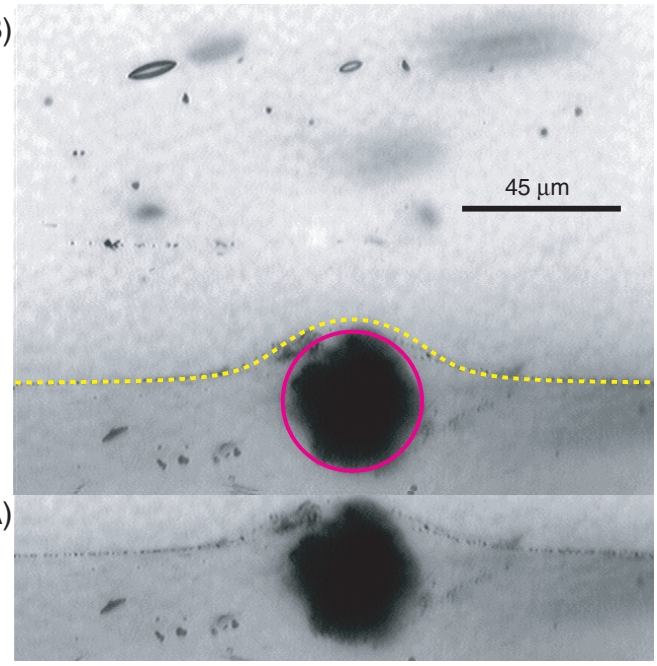

Figure 7. (A) Trail of small oxide particles deformed by flow around a large cluster of oxide particles. (B) Predicted band shapes for simple shear (yellow) and pure shear (magenta) around a free-rotating sphere. B also shows deformed bubbles, the orientations of which, relative to the line of oxide particles, are consistent with a flow dominated by simple shear. Sample is from Rock Mesa, Oregon, USA (Rust et al., 2003). Thick black line shows the boundary between the cluster of particles and glass.

CONCLUDING REMARKS

The pattern of band deformation around solid inclusions provides constraints on the dominant style of flow experienced by the lava. Deformed bands around bubbles are not useful for quantifying dynamics and kinematics other than verifying the obvious: bands are indeed shaped by flow. Features other than deformed bands, such as deformed bubbles, enclaves, fabrics, and folds, provide complementary information about kinematics and dynamics. Integrating constraints from deformed bands can thus provide either new information or independent tests of inferences.

ACKNOWLEDGMENTS

I thank J.V. Smith, G. Ventura, J. Castro, H.M. Gonnermann, A.C. Rust, M. Pompilio, and A. Wenzel for comments and suggestions. This work was supported by the National Science Foundation.

REFERENCES CITED

Arbaret, L., Diot, H., and Bouchez, J.-L., 1996, Shape fabrics of particles in low concentration suspensions: 2D analogue experiments and application to tiling in magma: Journal of Structural Geology, v. 18, p. 941–950, doi: 10.1016/0191-8141(96)00011-9.

Biot, M.A., 1961, Theory of folding of stratified viscoelastic media and its implications in tectonics and orogenesis: Geological Society of America Bulletin, v. 72, p. 1595–1620.

Blake, S., and Fink, J.H., 2000, On the deformation and freezing of enclaves during magma mixing: Journal of Volcanology and Geothermal Research, v. 95, p. 1–8, doi: 10.1016/S0377-0273(99)00129-8.

Buisson, C., and Merle, O., 2004, Numerical simulation of strain within lava domes: Journal of Structural Geology, v. 26, p. 847–853, doi: 10.1016/j.jsg.2003.11.017.

Castro, J.M., 1999, Textural and structural development of obsidian lavas [Ph.D. thesis]: Eugene, University of Oregon, 161 p.

Castro, J.M., and Cashman, K.V., 1999, Constraints on rheology of obsidian lavas based on mesoscopic folds: Journal of Structural Geology, v. 21, p. 807–819, doi: 10.1016/S0191-8141(99)00070-X.

Castro, J.M., Manga, M., and Cashman, K.V., 2002, The emplacement of Obsidian Dome, California: Insights from measurements of crystal orientation: Earth and Planetary Science Letters, v. 199, p. 211–226, doi: 10.1016/S0012-821X(02)00559-9.

Castro, J.M., Cashman, K.V., and Manga, M., 2003, A technique for measuring 3-D crystal-size distributions of prismatic microlites in obsidian: American Mineralogist, v. 88, p. 1230–1240.

Coward, M.P., 1980, The analysis of flow profiles in a basaltic dyke using strained vesicles: Geological Society of London Journal, v. 137, p. 605–615.

Donnelly-Nolan, J.M., Champion, D.E., Miller, C.D., Grove, T.L., and Trimble, D.A., 1990, Post-11,000-year volcanism at Medicine Lake Volcano, Cascade Range, northern California: Journal of Geophysical Research, v. 95, p. 19,693–19,704.

Eichelberger, J.C., Carrigan, C.R., Westrich, H.R., and Price, R.H., 1986, Non-explosive silicic volcanism: Nature, v. 323, p. 598–602, doi: 10.1038/323598a0.

Fink, J.H., 1980, Surface folding and viscosity of rhyolite flows: Geology, v. 8, p. 250–254, doi: 10.1130/0091-7613(1980)8<250:SFAVOR>2.0.CO;2.

Fink, J.H., Anderson, S.W., and Manley, C.R., 1992, Textural constraints on effusive silicic volcanism: Beyond the permeable foam model: Journal of Geophysical Research, v. 97, p. 77–88.

Gonnermann, H.M., and Manga, M., 2003, Explosive volcanism may not be an inevitable consequence of magma fragmentation: Nature, v. 426, p. 432–435, doi: 10.1038/nature02138.

Gonnermann, H.M., and Manga, M., 2005, Flow banding in obsidian: A record of evolving textual heterogeneity during magma deformation: Earth and Planetary Science Letters, v. 236, p. 135–147.

Gray, N.H., Philpotts, A.R., and Dickson, L.D., 2003, Quantitative measures of textural anisotropy resulting from magmatic compaction illustrated by a sample from the Palisades sill, New Jersey: Journal of Volcanology and Geothermal Research, v. 121, p. 293–312, doi: 10.1016/S0377-0273(02)00463-8.

Holtz, F., Lenne, S., Ventura, G., Vetere, F., and Wolf, P., 2004, Non-linear deformation and break up of enclaves in a rhyolitic magma: A case study from Lipari Island (southern Italy): Geophysical Research Letters, v. 31, p. L24611, doi: 10.1029/2004GL021590.

Leal, L.G., 1992, Laminar flow and convective transport processes: Boston, Butterworth-Heineman, 740 p.

Manga, M., 1998, Orientation distribution of microlites in obsidian: Journal of Volcanology and Geothermal Research, v. 86, p. 107–115, doi: 10.1016/S0377-0273(98)00084-5.

Manga, M., Castro, J., Cashman, K.V., and Loewenberg, M., 1998, Rheology of bubble-bearing magmas: Journal of Volcanology and Geothermal Research, v. 87, p. 15–28, doi: 10.1016/S0377-0273(98)00091-2.

McKenzie, D., and Holness, M., 2000, Local deformation in compacting flows: Development of pressure shadows: Earth and Planetary Science Letters, v. 180, p. 169–184, doi: 10.1016/S0012-821X(00)00152-7.

Merle, O., 1998, Internal strain within lava flows from analogue modelling: Journal of Volcanology and Geothermal Research, v. 81, p. 189–206, doi: 10.1016/S0377-0273(98)00009-2.

Miller, C.D., 1985, Holocene eruptions at the Inyon volcanic chain, California: Implications for possible eruptions in Long Valley Caldera: Geology, v. 13, p. 14–17, doi: 10.1130/0091-7613(1985)13<14:HEATIV>2.0.CO;2.

Paterson, S.R., Pignotta, G.S., and Vernon, R.H., 2004, The significance of microgranitoid enclave shapes and orientations: Journal of Structural Geology, v. 26, p. 1465–1481, doi: 10.1016/j.jsg.2003.08.013.

Perugini, D., Ventura, G., Petrelli, A., and Poli, G., 2004, Kinematic significance of morphological structures generated by mixing of magmas: A case study from Salina Island (southern Italy): Earth and Planetary Science Letters, v. 222, p. 1051–1066, doi: 10.1016/j.epsl.2004.03.038.

Polacci, M., and Papale, P., 1997, The evolution of lava flows from ephemeral vents at Mount Etna: Insights from vesicle distribution and morphological studies: Journal of Volcanology and Geothermal Research, v. 76, p. 1–17, doi: 10.1016/S0377-0273(96)00070-4.

Rust, A.C., and Manga, M., 2002, Orientation and deformation of bubbles in shear flows: Journal of Colloid and Interface Science, v. 249, p. 476–480, doi: 10.1006/jcis.2002.8292.

Rust, A.C., Manga, M., and Cashman, K.V., 2003, Determining flow type, shear rate and shear stress in magmas from bubbles shapes and orientations: Journal of Volcanology and Geothermal Research, v. 122, p. 111–132, doi: 10.1016/S0377-0273(02)00487-0.

Saar, M.O., Manga, M., Cashman, K.V., and Fremouw, S., 2001, Numerical simulations of the onset of yield strength in crystal-melt suspensions: Earth and Planetary Science Letters, v. 187, p. 367–379, doi: 10.1016/S0012-821X(01)00289-8.

Schmalholz, S.M., and Podladchikov, Y.Y., 2000, Finite amplitude folding: Transition from exponential to layer length controlled growth: Earth and Planetary Science Letters, v. 179, p. 363–377, doi: 10.1016/S0012-821X(00)00116-3.

Scott, W.E., 1987, Holocene rhyodacite eruptions on the flanks of South Sister Volcano, Oregon, *in* Fink, J.H., The emplacement of silicic domes and lava flows: Geological Society of America Special Paper 212, p. 35–53.

Seaman, S.J., 1995, Multi-stage magma mixing and mingling and the origin of flow banding in the Aliso Lava Dome, Tumacacori Mountains, southern Arizona: Journal of Geophysical Research, v. 100, p. 8381–8398, doi: 10.1029/94JB03260.

Shelley, D., 1985, Determining paleo-flow directions from groundmass fabrics in the Lyttleton radial dykes, New Zealand: Journal of Volcanology and Geothermal Research, v. 25, p. 69–79, doi: 10.1016/0377-0273(85)90005-8.

Smith, J.V., 1996, Ductile-brittle transition structures in the basal shear zone of a rhyolite lava flow, eastern Australia: Journal of Volcanology and Geothermal Research, v. 72, p. 217–223, doi: 10.1016/0377-0273(96)00009-1.

Smith, J.V., 2000, Textural evidence for dilatant (shear thickening) rheology of magma at high crystal concentrations: Journal of Volcanology and Geothermal Research, v. 99, p. 1–7, doi: 10.1016/S0377-0273(99)00191-2.

Smith, J.V., 2002, Structural analysis of flow-related textures in lavas: Earth-Science Reviews, v. 57, p. 279–297, doi: 10.1016/S0012-8252(01)00081-2.

Smith, J.V., and Houston, H.C., 1994, Folds produced by gravity spreading of a banded rhyolite lava flow: Journal of Volcanology and Geothermal Research, v. 63, p. 89–94, doi: 10.1016/0377-0273(94)90019-1.

Stevenson, R.J., Briggs, R.M., and Hodder, P.W., 1993, Emplacement history of a low-viscosity, fountain-fed pantelleritic lava flow: Journal of Volcanology and Geothermal Research, v. 57, p. 39–56, doi: 10.1016/0377-0273(93)90030-U.

Tuffen, H., Dingwell, D.B., and Pinkerton, H., 2003, Repeated fracture and healing of silicic magma generate flow banding and earthquakes?: Geology, v. 31, p. 1089–1092, doi: 10.1130/G19777.1.

Ventura, G., 2001, The strain path and emplacement mechanism of lava flows; an example from Salina (southern Tyrrhenian Sea, Italy): Earth and Planetary Science Letters, v. 188, p. 229–240, doi: 10.1016/S0012-821X(01)00299-0.

Ventura, G., De Rosa, R., Colletta, E., and Mazzuoli, R., 1996, Deformation patterns in a high-viscosity lava flow inferred from the crystal preferred orientation and imbrication structures: An example from Salina: Bulletin of Volcanology, v. 57, p. 555–562.

Wada, Y., 1992, Magma flow directions inferred from preferred orientations of phenocrysts in a composite feeder dike, Mikaye-Jima, Japan: Journal of Volcanology and Geothermal Research, v. 49, p. 119–126, doi: 10.1016/0377-0273(92)90008-2.

Webb, S.L., and Dingwell, D.B., 1990, Non-Newtonian rheology of igneous melts at high stresses and strain rates; experimental results for rhyolite, andesite, basalt, and nephelinite: Journal of Geophysical Research, v. 95, p. 15,695–15,701.

Williams, Q., and Tobisch, O.T., 1994, Microgranitic enclave shapes and magmatic strain histories: Constraints from drop deformation theory: Journal of Geophysical Research, v. 99, p. 24,359–24,368, doi: 10.1029/94JB01940.

Manuscript Accepted by the Society 19 April 2005